

DAMAGE DETECTION IN A HELICOPTER ROTOR BY ADAPTIVE ESTIMATION

Jonathan Alkahe*

Omri Rand†

Yaakov Oshman‡

Technion – Israel Institute of Technology
Department of Aerospace Engineering
Haifa 32000, Israel

Abstract

A new approach for detection and identification of damage in a rotating helicopter rotor is presented. A full-scale rotor analysis has been carried out using a detailed model of the blade elastic behavior and dynamics, where the blade elastic modes in addition to root hinge rotational degrees of freedom comprise a state vector. Several damage locations are considered and a set of Kalman filters is constructed accordingly. The best fitting model, according to measurements taken from the truth model, is determined in a probabilistic manner. In the proposed approach, measurement and process noise are treated inherently, enabling enhanced performance compared to other published methods. Combined with the model-based feature, the proposed algorithm eliminates the need for a training stage and enables a wide range of flight regimes. In this work, noisy measurements are generated using sensors placed at a finite element node along the blade. A Monte-Carlo analysis is carried out, giving a comprehensive view of the statistical nature of the results. A parametric study is presented and conclusions concerning the detectability of damage in a helicopter rotor and the efficiency of the proposed method are drawn.

1. Introduction

The detection of damage as a part of self health monitoring in structural systems is an important contributor to their safety, reliability and structural integrity. Early damage detection has the potential of reducing life cycle costs and possibly increasing replacement time intervals. If damage is located and monitored, then components of the structure may be replaced before some critical

point is reached and a dangerous failure occurs.

Cracks found in structural elements have various causes. One form of cracks is caused by fatigue and takes place under service conditions as a result of the limited fatigue strength. Cracks may also appear due to mechanical defects or manufacturing processes. Cracks present a serious threat to proper performance and most failures of presently used equipment are due to material fatigue. For this reason, methods enabling early detection and localization of cracks have been the subject of many studies.¹⁻⁵

One class of damage detection methods in which damage is seen as a change in the parameters of a structural model is based on modal information. Typically, modal-based damage detection methods use a finite element model of the system combined with experimental modal data to determine damage location and extent. The effect of cracks on the natural frequencies of a cantilever beam is demonstrated in Ref. 2. In their study, the authors assumed that the cracks occur in the first mode of fracture: i.e., the crack opening mode. These cracks were modeled using rotational springs with equivalent stiffnesses. The natural frequencies were calculated by solving the beam's deflection partial differential equation with the appropriate boundary conditions at the crack locations. The positions of two cracks in relation to each other, in addition to the changes in crack depths, was shown to affect the beam's natural frequencies. However, only the first mode was shown, and no information was given regarding the effect of the cracks relative to an undamaged beam. The work presented in Ref. 3 also applies a rotational spring to model the crack when the crack is open. The crack parameters (size and location) are to be extracted by examining two crack signatures calculated by subjecting the beam to harmonic loading at two frequencies that would excite the first and second modes. These crack signatures are calculated using Fourier transforms of the displacement at a specific point along the beam, and are shown to

*Graduate Student.

†Associate Professor.

‡Associate Professor.

Presented at the 26th European Rotorcraft Forum, 26-29 September 2000, The Hague, The Netherlands.

be very small. Since natural frequencies change very slightly as crack size and location varies, the addition of noise, not treated in this work, would significantly decrease the identification capability. In Ref. 4 the changes in mode shape due to presence of structural damage was determined. A finite element model with reductions of the modulus of elasticity in prescribed segments was implemented. It was shown that the elastic rotation undergoes a step jump in value when crossing the damage location, while the displacement parameter takes a change in its slope. An eigenstructure assignment technique for damage detection in rotating structures is demonstrated in Ref. 5. The damage is simulated by a 10% loss of mass and stiffness in the damaged element. The eigenvector that best approximates the damaged eigenvector is obtained and the angle between these two vectors is evaluated. This process is repeated for every one of the modes considered. A test case with noise contaminated mode shapes is also presented. An extension to this algorithm for rotating helicopter blades accounting for hovering aerodynamics is presented in Ref. 6. The blade's aerodynamics is incorporated as a damping term in the structural dynamics of the blade. The damage is shown to be properly characterized when flapping modes are used. However, the algorithm presented is based on taking the pseudo-inverse of a known matrix in order to solve for the damage extent. This key component, actually, is a least-squares estimation procedure which could prove to be very poor in some cases.

Another approach for damage detection in beam structures described in literature is using a subspace rotation algorithm.¹ This method views damage location and damage extent as two different problems requiring two separate solutions. In this approach, damage is manifested as changes in the mass, damping and stiffness matrices of the structure. Strain sensors were used, therefore, a method for extracting displacement frequency responses from strain data was presented. This study shows that higher-order vibration modes are required to locate damage events. In addition, condensation methods can not be used to remove rotational degrees of freedom because of their coupling with translation degrees of freedom.

Several studies have been published concerning damage detection in helicopters.⁷⁻¹⁰ In these works, a model of the helicopter is utilized to simulate typical main rotor components faults. The model results are then inserted as inputs to a neural network in order to complete the training stage. The network's detection capability is tested in several cases including noise corrupted

inputs.

In the present study, the damage detection methodology is based on the multiple-model approach. In this method various damage locations and levels are considered, where each case is adequately represented by a finite element model. A Kalman filter is tuned according to each model and the best fitting one is determined in a probabilistic manner based on noisy displacement or velocity measurements. Previous studies concerning a rotating blade can be found in Refs. 11, 12. The results in these works have clearly demonstrated high damage detection and identification capability. In addition, an extensive parametric study was carried out, giving insight on the influence of various parameters.

2. The Multiple-Model Adaptive Estimation approach

In various estimation problems, specifically in damage detection cases, uncertain parameters exist within the system model used for algorithm design. Typically, these parameters can undergo large jump changes. Such problems give rise to the need for the estimation of parameter values simultaneously with estimation of state variables. One means of accomplishing this is the multiple model adaptive estimation technique (MMAE).^{13,14} The system is assumed to be adequately represented by a linear stochastic state model, with uncertain parameters affecting the matrices defining the structure of the model or the noise distribution model. It is further assumed that the parameters can take only discrete values. In cases where continuous parameter values are presented, representative discrete values have to be chosen throughout the continuous range of possible values. A Kalman filter is then designed for each choice of parameter value, resulting in a bank of K separate filters. Based on the residuals of each one of these K filters, the conditional probabilities of each discrete parameter value being "correct" (given the measurement history to that time) are evaluated iteratively.

Following the development presented in Refs. 14, 15, consider the system model described by the first-order, linear, stochastic differential state equation of the form:

$$\dot{\mathbf{x}}(t) = \mathbf{F}(\mathbf{a})\mathbf{x}(t) + \mathbf{G}(\mathbf{a})\mathbf{w}(t) \quad (1)$$

with noisy measurements described by

$$\mathbf{z}(t_i) = \mathbf{C}(\mathbf{a})\mathbf{x}(t_i) + \mathbf{v}(t_i) \quad (2)$$

where $\mathbf{x}(t)$ is the system state vector and $\mathbf{z}(t)$ is the measurement vector. It is assumed that $\mathbf{w}(t)$ and $\mathbf{v}(t)$ are independent, zero-mean, white

Gaussian noise processes with covariances $\mathbf{Q}(t)$ and $\mathbf{R}(t)$, respectively. \mathbf{a} is a vector containing all the uncertain dynamic parameters given in the system model. $\mathbf{F}(\mathbf{a})$ is the system plant matrix, $\mathbf{G}(\mathbf{a})$ is the noise distribution matrix and $\mathbf{C}(\mathbf{a})$ is the measurement matrix. Since \mathbf{a} may assume a continuous range of values over the space of allowable parameters, it is necessary to discretize \mathbf{a} into a set of J vector values: $\mathbf{a}_1, \mathbf{a}_2, \dots, \mathbf{a}_J$. A multiple model adaptive estimator consists of J independent Kalman filters, in which the j th filter is constructed according to a specific parameter set \mathbf{a}_j . These J filters form a bank of elemental filters which are processed in parallel. Each elemental filter produces its own estimate of the true state, denoted as $\hat{\mathbf{x}}_j(t_i)$, for the j th hypothesized value of \mathbf{a} . The residuals of all J elemental filters are then used to calculate the probability that \mathbf{a} assumes the value \mathbf{a}_j at time t_i , for $j = 1, 2, \dots, J$. This probability is called the ‘‘hypothesis conditional probability’’ and is denoted as $p_j(t_i)$. This conditional probability represents the validity of the j th filter’s system model at time t_i . The hypothesis conditional probabilities $p_j(t_i), j = 1, 2, \dots, J$, are calculated at each sample time t_i , by the recursive equation:

$$p_j(t_i) = \frac{f_{\mathbf{z}(t_i|\mathbf{a}, \mathbf{Z}(t_{i-1}))}(\mathbf{z}_i|\mathbf{a}_j, \mathbf{Z}_{i-1}) p_j(t_{i-1})}{\sum_{k=1}^J f_{\mathbf{z}(t_i|\mathbf{a}, \mathbf{Z}(t_{i-1}))}(\mathbf{z}_i|\mathbf{a}_k, \mathbf{Z}_{i-1}) p_k(t_{i-1})} \quad (3)$$

where $\mathbf{Z}(t_{i-1})$ is the measurement history from the first sample time until sample time t_{i-1} , and the innovation probability density function is given by

$$f_{\mathbf{z}(t_i|\mathbf{a}, \mathbf{Z}(t_{i-1}))}(\mathbf{z}_i|\mathbf{a}_j, \mathbf{Z}_{i-1}) = \frac{1}{(2\pi)^{S/2} |\mathbf{A}_k(t_i)|^{1/2}} \cdot \exp \left\{ -\frac{1}{2} \mathbf{r}_k^T(t_i) \mathbf{A}_k^{-1}(t_i) \mathbf{r}_k(t_i) \right\} \quad (4)$$

where S is the number of sensors. The k th filter residual vector is:

$$\mathbf{r}_k(t_i) = \mathbf{z}(t_i) - \mathbf{H}_k(t_i) \hat{\mathbf{x}}_k(t_i^-) \quad (5)$$

where $\hat{\mathbf{x}}_k(t_i^-)$ is the k th filter predicted state estimate. The k th filter-computed residual covariance matrix, $\mathbf{A}_k(t_i)$ is calculated by

$$\mathbf{A}_k(t_i) = \mathbf{H}_k(t_i) \mathbf{P}_k(t_i^-) \mathbf{H}_k^T(t_i) + \mathbf{R}_k(t_i) \quad (6)$$

where $\mathbf{P}_k(t_i^-)$ is the k th filter prediction error covariance. The residual of the j th filter plays a major role in determining $p_j(t_i)$. As is evident from (3), the filter with the smallest value of $\mathbf{r}_j^T(t_i) \mathbf{A}_j^{-1}(t_i) \mathbf{r}_j(t_i)$ assumes the largest conditional hypothesis probability. Thus, this algorithm is consistent with the intuition that the residuals of a well-matched filter should be

smaller (relative to the filter’s internally computed residual covariance, \mathbf{A}_j) than the residuals of a mismatched filter. To allow the estimator to adapt to the changing parameter value, the hypothesis conditional probabilities are artificially bounded below by a small number (0.0005). This insures preventing any of them from converging to zero, which would make it very difficult for them to change significantly in response to a subsequent change in true parameter value.

3. Structural Model

The full-scale rotor analysis has been carried out using the software package RAPID/Plus,¹⁶ which is capable of modeling general rotorcraft configurations, conventional helicopters and tilt-rotors. RAPID/Plus may handle nonuniform and dissimilar blades and is therefore suitable to the current task. Both rigid and elastic blade analyses are possible. Blade elasticity is modeled using a built-in modal based analysis for structurally pretwisted spars. This analysis enables including the blade’s axial, lead-lag, flap and twist elastic deformations, designated by u, v, w and ϕ , respectively. Damage is manifested through a reduction in the bending stiffnesses and torsional rigidity of one element at a specific location along the span. Calculation of the reduced stiffness caused by a crack, based on fracture mechanics concepts, can be found in Refs. 3, 11. A deformed blade is presented in Fig. 1. The model also includes fully articulated blades with arbitrary pitch, flap and lag offsets, root springs and dampers, and a detailed control system mechanism (swashplate, elastic pitch links, pitch horn, etc.), which enables future study of faults in these components.

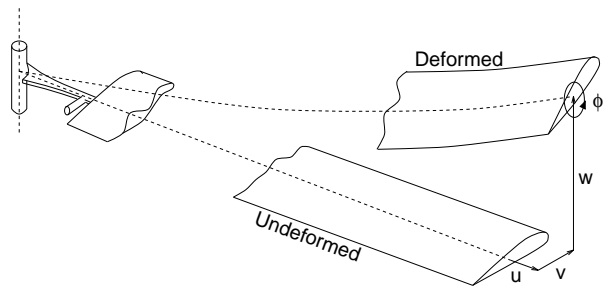


Figure 1: A deformed elastic blade

The damage detection algorithm consists of 5 different models running in parallel – 4 damaged blade models along with the baseline undamaged blade model. These models are designated as ‘‘0’’ for the baseline model and ‘‘1’’–‘‘4’’ for the damaged blade models. The modeled

damage, reflected by reduced stiffness values, is assumed to be located at one of four spanwise locations designated by $x/R = 0.15, 0.35, 0.55$ and $x/R = 0.75$. The true damage may occur at 10 equally spaced elements along the blade (i.e. $x/R = 0.1, 0.2, \dots, 1.0$).

3.1 Damage Identification Logic

The decision logic is based on calculating the fitness probability for each of the models over an inspection time interval (designated as t_d). Let $p_j(t_i)$ denote the hypothesis conditional probability of the j th model at a discrete time t_i (3), and q_j refer to the fitness probability of the j th model. Then

$$q_j = \frac{\sum_{t \in t_d} p_j(t)}{\sum_{k=1}^J \sum_{t \in t_d} p_k(t)} \quad (7)$$

Let q_{max} be defined as

$$q_{max} \triangleq \max_{j \in \{1, 2, \dots, J\}} \{q_j\} \quad (8)$$

The model associated with q_{max} is said to describe the true damaged behavior in the best manner. In order to provide a comprehensive view of the statistical nature of the results, a Monte-Carlo analysis¹⁷ is carried out, where the same damaged case is repeated. For each one of the tested cases, the Monte-Carlo procedure continues until no change occurs in the model found to be the most fitting, and its identification probability, or a limit of 150 runs is reached.

4. Parametric Study

The detection and identification capabilities of the proposed method are demonstrated through two test cases of a full-scale, fixed-shaft rotor with flap, lead-lag and twist elastic motions.

4.1 In vacuum results

Consider a two-bladed fixed-shaft rotor in vacuum with blade properties listed in Table 1. In this case, 3 elastic modes are considered: the first beamwise (flap) bending mode, the first chordwise (lead-lag) bending mode and the first twist mode. Here, the damage is manifested as a 10% reduction in both the beamwise and the chordwise stiffnesses, as well as in the torsional rigidity, at a specific blade element. The equations of blade motions are derived using RAPID/Plus.¹⁶ The system matrices are then utilized for constructing the bank of Kalman filters. In this case the damaged models are spread along the blade as previously stated in section 3., however, the damage is assumed to occur only in one of the

blades – designated as blade#1. Moreover, the models account for damage only in blade#1.

Three measurements are taken at a specific node along blade#1 – two velocity components (vertical and horizontal), and one angular velocity (pitch rate). The measurement noise standard deviation is ± 0.1 m/s for velocity and ± 0.1 rad/s for angular velocity (these values correspond to a signal to noise ratio of 10 for measurements taken at the blade’s tip). For this case, 4 rotor revolutions are taken as the detection time interval, while the decision time is the last revolution. Since there are 11 possible locations of the true damage (zero means no damage), and 10 different sensor locations, the total number of cases inspected equals 110. In Figs. 2, 3, 4 three performance measures of the proposed detection and identification algorithm are examined: False alarm, missed detection and false identification rates, all presented versus sensor location along the blade. False alarm rate is defined as the probability of detecting damage when no damage occurs. Missed detection is the probability of obtaining the output “no damage” while damage indeed occurs along the blade. The case of false identification is defined, in this study, as the probability of detecting true damage, albeit in a wrong location. Fig. 5 shows the damage identification results. The shaded areas in Fig. 5 comprise all the cases in which the *true damage was identified* (this is the case where the model associated with q_{max} represents damage location closest to the true damage location). The first column (zero damage location) represents the no-damage case. Let p denote the probability of a correct identification for a specific damage and sensor locations, defined as $p \triangleq \frac{N_c}{N_{MC}}$ where N_c corresponds to the number of Monte-Carlo runs in which correct identification was achieved, and N_{MC} is the total number of Monte-Carlo runs. Three levels of confidence are shown, each one corresponding to an interval of values of p . Let \bar{q}_{max} be defined as

$$\bar{q}_{max} \triangleq \begin{cases} q_{max} & \text{correct identification achieved,} \\ 0 & \text{no identification.} \end{cases} \quad (9)$$

then the percentage given in Fig. 5 is given by:

$$\text{True ID} = \frac{\sum_{x_d=0}^1 \sum_{x_s=0.1}^1 \bar{q}_{max}(x_d, x_s)}{110} \quad (10)$$

where x_d is the damage location, x_s refers to the sensor location, and $\bar{q}_{max}(x_d, x_s)$ is computed according to Eqs. 8, 9. As demonstrated, damage detectability, using the proposed method, is fairly high at most sensor locations. The high false alarm rate, for sensors located near the blade’s root, originates from the relatively low signal

Table 1: Rotor properties.

Radius	$R = 8.2 \text{ m}$
Chord	$c = 0.53 \text{ m}$
Beamwise stiffness	$EI_b = 7.62 \cdot 10^4 \text{ Nm}^2$
Chordwise stiffness	$EI_c = 1.72 \cdot 10^5 \text{ Nm}^2$
Torsional rigidity	$GJ = 8.57 \cdot 10^4 \text{ Nm}^2$
Tensile stiffness	$AE = 2.97 \cdot 10^9 \text{ N}$
Mass per unit length	$\lambda = 10 \text{ Kg/m}$
Angular velocity	$\Omega = 27 \text{ rad/s}$

to noise ratio (10 at tip, less than 10 inboard) adopted in the present results.

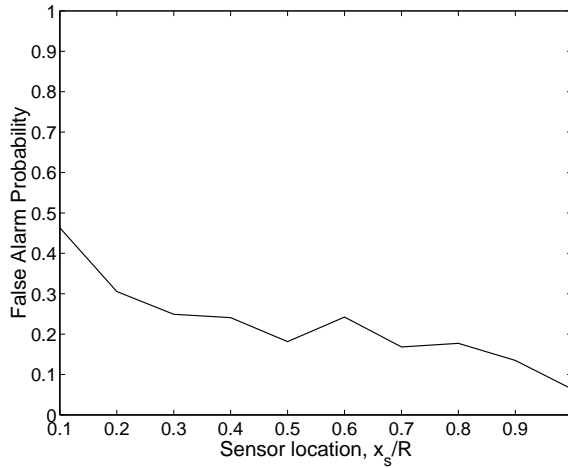


Figure 2: False alarm rate.

4.2 Aerodynamics included results

Consider the same rotor as discussed in the previous section. In this case aerodynamic loads are also presented, and therefore, a trim (equilibrium) state has to be determined initially. The blades are given collective and cyclic commands and the periodic steady-state response is calculated for each one of the 5 models. The state vector now comprises of 5 coupled elastic modes, which include the first 2 flap modes, first 2 lead-lag modes and the first pitch elastic mode. In order to stabilize the unstable lead-lag modes a damper is introduced and the lead-lag root angle is added to the state vector. The measurements

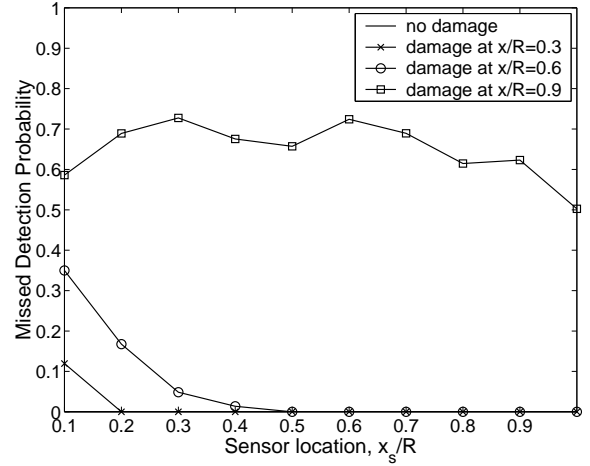


Figure 3: Missed detection probability.

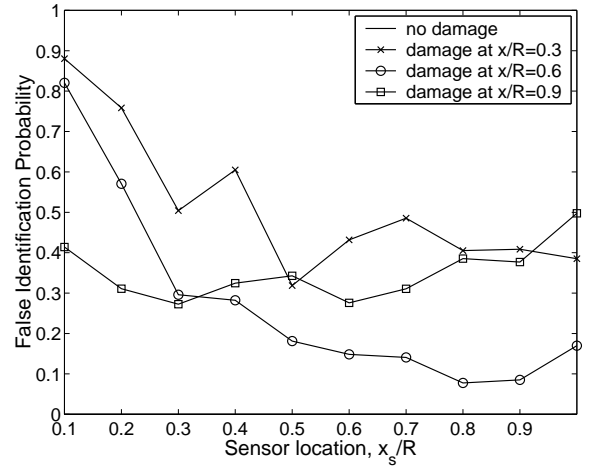


Figure 4: False identification probability.

taken include beamwise and chordwise velocities along with the pitch rate *at the tip of the two blades*. Since the rotor blades now respond basically in a periodic manner, the measurement vector includes, along with response to initial conditions, the true periodic response. In order to include in the filtering algorithm only the differences between the various models, the measurements are pre-processed in each filter. In this preliminary stage, the current filter *calculated* periodic response is subtracted from the measurements. Therefore, the measurements embedded information consists of small deviations from periodic response due to initial conditions, in addition to small steady-state response differences between the various models and the truth model. Owing to the zero external excitation, the detection and identification process is based solely on these small steady-state differences, combined with small changes in modal shapes and natural frequencies.

In the case under discussion, the true damage

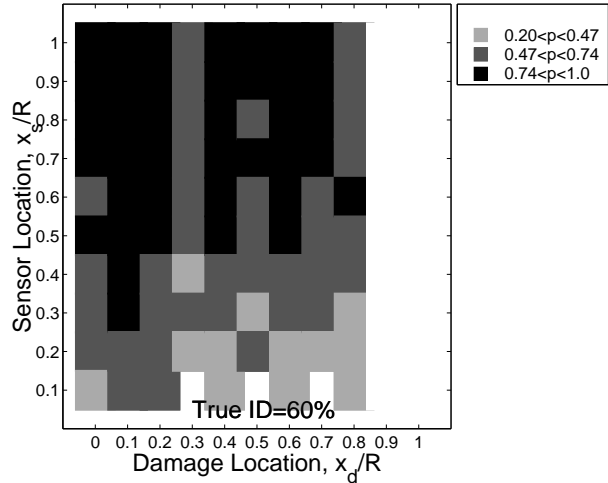


Figure 5: In vacuum rotor damage identification results

is located at $x/R = 0.2$ where x is measured from the blade's root. Two damage levels are presented in the damaged models: the first damage intensity is manifested as a 30% stiffness reduction and the second level is represented by a 45% reduction. Moreover, 2 noise levels are introduced through the noise percentage: a low noise level represented as 0.2% of the measurement, and a second level of 1%.

Fig. 6 shows the detection probability for the various damage and noise levels, defined as the probability to detect actual damage occurring (regardless the damage location). Clearly, high detection capability is demonstrated for 0.2% noise level, while a noise level of 1% causes a substantial reduction of this capability. This is due to the lack of sufficient difference between the damaged and undamaged models. Thus, the results for the 0.2% noise level show that the present approach is capable of distinguishing between very similar models, while the effects of a noise level of 1% are equivalent to the differences between the models and therefore cause the presented degradation in damage detectability. It should also be noted that the undamaged and the damaged models are based on modal representation of the Finite-Element modeling. While, such an approach contributes to the efficiency of the numerical procedure, it tends to “smooth” the differences between the models.

Fig. 7 shows the true identification probability, meaning the location of the identified model is indeed the closest to the actual damage location (in this study, the model expected to be identified is the one related to $x/R = 0.15$). For

the larger damage level (45%) and 0.2% noise the true location is identified with a relatively high probability. In the other cases damage is still detected, however the identified model location is not the closest to the true one. This miss-identification is caused again by the proximity of one damaged model to another.

Fig. 8 demonstrates the false alarm probability vs. modeled damage level for the various noise levels. In the case where a 30% stiffnesses reduction is implemented in the four damaged models a relatively high false alarm rate exists. Since this rate is equivalent to the miss-identification of the undamaged model, when indeed no damage occurs, a similar identification problem exists here as appeared also in Fig. 7. The very small differences between the five models (including the undamaged model) which are obtained for low damage levels, obscure the correct identification of the *undamaged* case. When a 45% damage level is implemented in the damaged models, and a low noise level is considered, the false alarm rate decreases to a lower, more acceptable, value of 0.14.

Adding aerodynamics tends to mask the influence of the reduced stiffnesses since high damping values are present. This causes the natural frequencies and modal shapes to become less sensitive to stiffness changes. Moreover, aerodynamics generates coupling between elastic modes, which is affected by stiffness changes, and ones which are hardly influenced. This effect also decreases damage detectability.

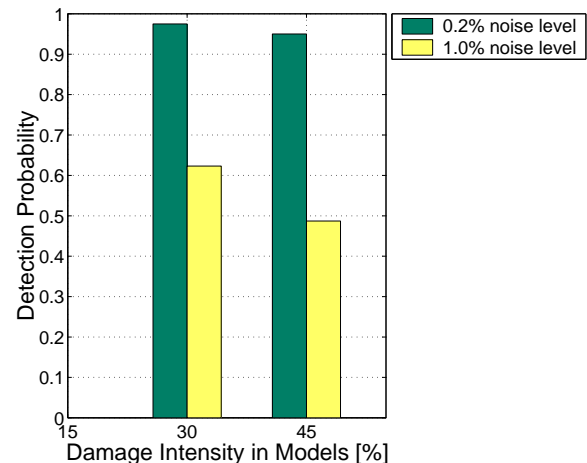


Figure 6: Detection probability for various noise and damage levels

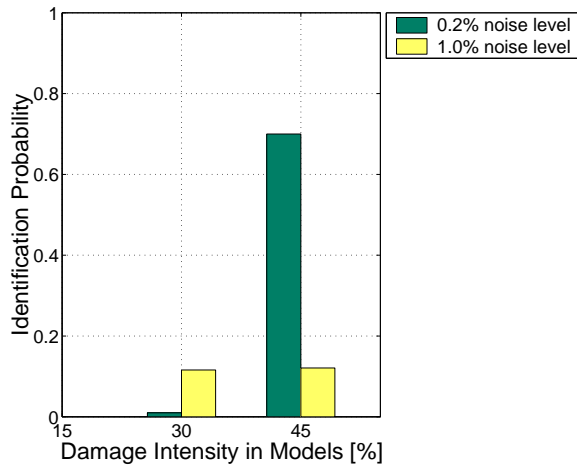


Figure 7: Identification probability for various noise and damage levels

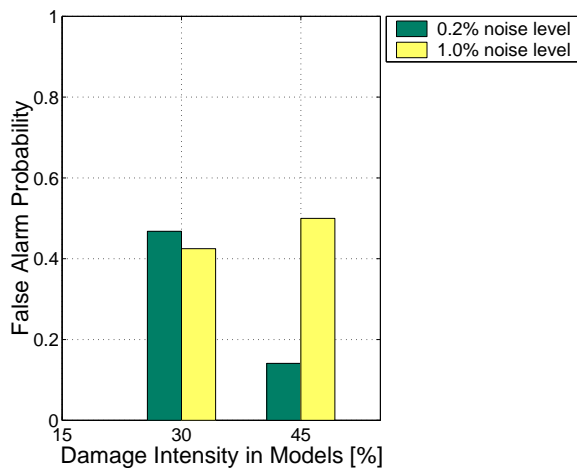


Figure 8: False alarm rate for various noise and damage levels

5. Conclusions

A model-based damage detection algorithm for a helicopter rotor, using an adaptive estimation technique, incorporating noisy measurements, is presented. The blade elastic and dynamic characteristics are introduced using RAPID/Plus package where finite element model of the blade is utilized to represent damage as equivalent reduced stiffnesses in one of the elements. A set of Kalman filters is constructed to simulate various damages. The proposed method enables various types of rotor faults and sensors to be implemented.

The algorithm presented constitutes a new approach towards damage detection in mechanical systems. Contrary to other model-based damage detection methods in helicopter rotors, such as methods based on neural networks, this

approach requires no training stage, and treats measurement and process noise inherently. The damage detection capability is tested in various cases. In general, for low noise levels, this approach produces good damage identification results. The results for the case of a full-scale rotor in vacuum clearly indicate good damage detectability although a relatively high noise level is present. When aerodynamics is present damage detectability generally deteriorates, due to damping and mode coupling. For 0.2% noise level and a relatively large stiffness reduction, fairly good detection and identification results are achieved.

As demonstrated in this work and also in other published studies, the problem of detecting and correctly locating local stiffness changes in helicopter rotor blades using noisy blade response measurements constitute a very difficult task. The significant advantage of the proposed approach arises from the filtering process enabling probabilistic determination based on relatively little information. Introducing an external excitation in this case would probably increase damage detectability since the transient system response will provide additional information. Moreover, other rotor faults such as blade mass changes, pitch link or damper defects, mistracking etc. are expected to be considerably more detectable. These topics are currently under investigation.

References

- 1 Kahl, K. and Sirkis, J. S., "Damage Detection in Beam Structures Using Subspace Rotation Algorithm with Strain Data," *AIAA Journal*, Vol. 34, No. 12, December 1996, pp. 2609–2614.
- 2 Ostachowicz, W. M. and Krawczuk, M., "Analysis of the Effect of Cracks on the Natural Frequencies of a Cantilever Beam," *Journal of Sound and Vibration*, Vol. 150, No. 2, 1991, pp. 191–201.
- 3 Sundermeyer, J. N. and Weaver, R. L., "On Crack Identification and Characterization In a Beam by Non-Linear Vibration Analysis," *Journal of Sound and Vibration*, Vol. 183, No. 5, 1995, pp. 857–871.
- 4 Yuen, M. M. F., "A Numerical Study of the Eigenparameters of a Damaged Cantilever," *Journal of Sound and Vibration*, Vol. 103, No. 3, 1985, pp. 301–310.
- 5 Kiddy, J. and Pines, D., "Eigenstructure Assignment Technique for Damage Detection in

- Rotating Structure,” *AIAA Journal*, Vol. 36, No. 9, September 1998, pp. 1680–1685.
- ⁶ Kiddy, J. and Pines, D., “The Effects of Aerodynamic Damping on Damage Detection in Helicopter Main Rotor Blades,” *54th Annual Forum of the American Helicopter Society*, Montreal, Canada, May 25–27 1999.
- ⁷ Ganguli, R. and Chopra, I., “Simulation of Helicopter Rotor-System Structural Damage, Blade Mistracking, Friction and Freeplay,” *Journal of the American Helicopter Society*, Vol. 35, No. 4, July 1998, pp. 591–597.
- ⁸ Stevens, P. W., Hall, D. L., and Smith, E. C., “A Multidisciplinary Research Approach to Rotorcraft Health and Usage Monitoring,” *52nd Annual Forum of the American Helicopter Society*, Washington, D.C., June 4–6 1996.
- ⁹ Hass, D. J. and Schaefer, C. G., “Emerging Technologies for Rotor System Health Monitoring,” *52nd Annual Forum of the American Helicopter Society*, Washington, D.C., June 4–6 1996.
- ¹⁰ Ganguli, R., Chopra, I., and Hass, D. J., “A Physics Based Model for Rotor System Health Monitoring,” *22nd European Rotorcraft Forum*, Brighton, UK, September 1996.
- ¹¹ Alkahe, J., Rand, O., and Oshman, Y., “Damage Detection in a Rotating Blade,” *40th Israel Annual Conference on Aerospace Sciences*, Haifa, Israel, February 23–24 2000.
- ¹² Alkahe, J., Rand, O., and Oshman, Y., “Damage Detection in a Rotating Helicopter Blade Using an Adaptive Estimator,” *AIAA/ Guidance, Navigation and Control Conference*, Denver, CO, August 14–17 2000.
- ¹³ Magill, D. T., “Optimal Adaptive Estimation of Sampled Stochastic Processes,” *IEEE Transactions on Automatic Control*, Vol. AC–10, No. 4, October 1965, pp. 434–439.
- ¹⁴ Maybeck, P. S., *Stochastic Models, Estimation, and Control*, Vol. 2, Academic Press, NY, 1982.
- ¹⁵ Stepaniac, M. J. and Maybeck, P. S., “MMAE-based Control Redistribution Applied to the VISTA F–16,” *IEEE Transactions on Aerospace and Electronic Systems*, Vol. 34, No. 4, October 1998, pp. 1249–1259.
- ¹⁶ Rand, O., “RAPID/Plus: Rotorcraft Analysis for Preliminary Design + Aeroelasticity: User Manual,” Tech. rep., Haifa, Israel, January 1999.
- ¹⁷ Freund, J. E., *Modern Elementary Statistics*, Prentice–Hall, New Jersey, 6th ed., 1984.